Sumer University Journal for Pure Science (ISSN: 2790-7031)
SUJPS 2023 (June), Vol. 2, No. 1, p.p.: 17-28

A simulation study of the applied voltage effect on the performance of electrostatic precipitators

Haidar K. Dhayef[1]*, Thamir H. Khalaf[2]

[1]College of Science, University of Sumer- IRAQ
[2]Department of physics, College of Science, University of Baghdad- IRAQ

Abstract

Electrostatic precipitators have been widely used in recent times to get rid of suspended dust in factory exhausts and chimneys. This is done by applying high voltage to the electrodes of the (wire-plate) precipitator under normal atmospheric pressure. When a voltage is applied to the internal electrodes (discharge electrodes), an irregular electric field results. The performance and efficiency of an ESP mainly depend on the voltage distribution and the applied electric field. The research project was implemented using a computer simulation method through the COMSOL Multiphysics program in a two-dimensional milieu. The effect of applied different voltages on internal discharge electrodes (20, 25, 30, 35 kV) on the performance and efficiency of the precipitator was studied. In this work, the cross-section of an electrostatic precipitator (wire- plate) was simulated using the finite element method (FEM). It was observed through the results that the dust particles accumulated on the collecting plates after they were charged through the precipitator channel increased with the increase of the applied voltage. Thus the efficiency increases dramatically reaching 100% at the applied voltage of 30 and 35 kV.

Keywords: Electrostatic precipitator, Corona discharge, Simulation, COMSOL Multiphysics software, Finite element method (FEM).

دراسة محاكاة لتأثير الجهد المطبق على أداء المرسبات الكهروستاتيكية

حيدر كريم ضايف[1]*, ثامر حميد خلف[2]

[1]كلية العلوم ,جامعة سومر , العراق

[2]قسم الفيزياء, كلية العلوم, جامعة بغداد, العراق

الخلاصة

تم استخدام المرسبات الكهروستاتيكية على نطاق واسع في الآونة الأخيرة للتخلص من الغبار العالق في عوادم المصنع والمداخن. يتم ذلك عن طريق تطبيق الجهد العالي على أقطاب المرسب (لوح الى أسلاك) تحت الضغط الجوي العادي. عندما يتم تطبيق الجهد على الأقطاب الكهربائية الداخلية (أقطاب التفريغ) ، ينتج مجال كهربائي غير منتظم. يعتمد أداء وكفاءة المرساب الكهروستاتيكي بشكل أساسي على توزيع الجهد المطبق والمجال الكهربائي. تم تنفيذ المشروع باستخدام طريقة المحاكاة الحاسوبية من خلال برنامج COMSOL Multiphysics في بيئة ثنائية الأبعاد. تمت دراسة تأثير الفولتية المطبقة على أقطاب التفريغ الداخلية (20 ، 25 ، 30 ، 35 ك.ف) على أداء وكفاءة المرسب. في هذا العمل ، تمت محاكاة المقطع العرضي للمرسب الكهروستاتيكي (لوح الى سلك) باستخدام طريقة العناصر المحدودة (FEM). لوحظ من خلال النتائج أن جزيئات الغبار المتراكمة على ألواح التجميع بعد شحنها من خلال قناة المرسب تزداد بزيادة الجهد المطبق. وبالتالي تزداد الكفاءة بشكل كبير لتصل إلى 100٪ عند الجهد المطبق 30 و 35 كيلو فولت.

* Haiderkareem@uos.edu.iq

1. Introduction

Today, the world is witnessing rapid technological development, and with this development, harmful emissions of micro and nanoparticles are increasing on the environment in general, and on human health in particular, and living organisms [1-4]. There are many invented technologies for filtering pollutants: among these are electrostatic precipitators. Precipitators are characterized by fluid flow through them and relatively good performance in the efficiency of collecting harmful particles and cleaning the air [5-7]. Electrostatic precipitators have many uses, all of which lie in the control of inlet gases for power generation plants., factory exhaust gases, combustion and chemical treatment units. It has been used mainly in the cleaning and purification of polluted air, which contains gases and various particulate matter [5,8]. Plate-wire type electrostatic precipitators have multiple uses and a wide range of applications. To solve the electric field detailed in the numerical study of the precipitator model requires the inclusion of particle transport and flow field modeling.

The basic operating mechanism for the performance of electrostatic precipitators is when gas molecules flow into its channel through high-voltage DC wires, the gas molecules ionize, allowing for the formation of a phenomenon called corona discharge in the enclosed region around the discharge wires. Volatile particles flowing through the precipitator channel are charged by the corona discharge, then attracted to the grounded electrodes (collecting plates) by Coulomb forces and trapped on them. The electrostatic deposition mechanism includes three basic steps:

- Particle charging
- particle aggregation
- Removing accumulated dust

When the electrostatic precipitator works, there are many factors that greatly affect its performance, and the applied voltage is one of the most important parameters because it determines the electrostatic field and thus discharges the corona (9,10). This research aims to provide a detailed two-dimensional simulation study of an electrostatic precipitator with different geometry and operational parameters as well as particle properties. And a study of the effect of the applied voltage on the discharge electrodes in order to obtain a high collection efficiency for the ESP wire-plate type.

2 Governing Equations:

The basic principles of operations within the ESP in the COMSOL software are divided into several physics modules: electrostatic laminar flow and particle tracking, where each module is solved separately.

2.1 Laminar Flow

Equation the Navier-Stokes is used to solve the pressure and velocity components within the ESP system[11]:

$$\rho(u\,.\nabla)u\,\nabla\; -\; \mathbf{pI}\;\boldsymbol{\mu}\,u\nabla\,(\nabla\mathbf{u})^{T} = \nabla.\,[\boldsymbol{\lambda}(\nabla\,.\,u)\mathbf{I}] +\; \boldsymbol{F_{EHD}} \qquad (1)$$

Where**:** $\boldsymbol{p}$ if the pressure (Pa), $\boldsymbol{\rho}$ is the fluid density (kg/m3), $\boldsymbol{\lambda}$ is bulk viscosity (kg/(m·s)), $\boldsymbol{\mu}$ is the dynamic viscosity (kg/(m·s)), $\mathbf{I}$ is matrix of one and $\mathbf{F_{EHD}}$ is the electro-hydrodynamic force define as

$$\mathrm{F_{EHD}} = \rho_q\, E \qquad (2)$$

The simulation is done by providing air properties from the base material library. The system temperature is set to room temperature, and the pressure is set to (1atm). The inputs are set as boundary conditions for the precipitator simulation system.

2.2 Electrostatics

In COMSOL Multiphysics® the electrostatic module solves the static electric field using Poisson's equation: [9].

$$\nabla . E = \rho_q / \varepsilon_0 \quad (3)$$

$$E = -\nabla V \quad (4)$$

$$\varepsilon_0 \nabla^2 V = -\rho_q \quad (5)$$

Where , **E** is the electric field, , $\boldsymbol{\varepsilon_0}$ is the vacuum permittivity, $\boldsymbol{\rho_q}$ (C/m3) the space charge number density, and $\boldsymbol{V}$ is electric potential, It is supposed to be applied to the internal electrodes of the precipitator system with a radius (0.5 mm). Previous work recorded the corona breakdown voltage value [11].

2.3 Particle tracing

By solving the second-order equations of motion according to Newton's second law of the body position vector components, the position of the particles is calculated. Particle migration velocity is also governed by Newton's second law of motion, which states that the force applied to an object is equal to the change in momentum of the object per unit time. And as follows:

$$\frac{dq}{dt} = v \quad (6)$$

$$\frac{d}{dt}(m_p v) = F_t \quad (7)$$

Where: $\boldsymbol{v}$ is the particle velocity (m/s), **q** is the particle position (m), $\boldsymbol{m_p}$is the particle mass (kg), and $\boldsymbol{F_t}$is the total force (N) acting on the particle. In this model there are two forces acting on the particles, the drag force and the electrostatic force, where the drag force $\boldsymbol{F_D}$ (N) is described as follows:

$$F_D = \frac{1}{\tau_p S} m_p (u - v) \quad (8)$$

Where $\boldsymbol{\tau_p}$ the particle velocity response time (s) define as:

$$\tau_p = \frac{4 \rho_p d_p^2}{3 \mu C_D Re_r} \quad (9)$$

Where $\boldsymbol{C_D}$ is the drag coefficient, $\boldsymbol{\rho_p}$is the density of the particles (kg/m^3), $\boldsymbol{d_p}$is the particle diameter (m), and $\boldsymbol{Re_r}$ is the relative Reynolds number given by the expression:

$$Re_r = \frac{\rho |u - v| d_p}{\mu} \quad (10)$$

and S is the drag correction coefficient defined as:

$$S = 1 + Kn\left(C_1 + C_2 exp\left(-\frac{C_3}{Kn}\right)\right) \quad (11)$$

where are dimensionless coefficients.

And $\boldsymbol{F_e}$ (N) is the electric force acting on the particles within the ionization space, and is defined as follows:

$$\overrightarrow{F_e} = eZ\overrightarrow{E} \quad (12)$$

Where The force vectors $\overrightarrow{\boldsymbol{F_e}}$ represents the Coulombs force, e (C) is the elementary charge, and Z is the accumulated charge number on each particle.

One of the methods of charging the particles to be collected is adopted: diffusion charging, field charging, and the charging mechanism based on the combination of the two previous methods. The variable ((eZ)) represents the charge of the particle, which depends on the residence time of the ionized gas, while the charge processes depend mainly on the size of the particle. [12].

According to the Lawless model, the accumulated charge can be calculated on the loaded particles inside the space of the ESP:

$$\tau_c \frac{dZ}{dt} = \begin{cases} R_f + f_a & (|v_e| \le |v_s|) \\ R_d f_a & (|v_e| > |v_s|) \end{cases} \quad (13)$$

where $\tau_c$is the characteristic charging time:

$$\tau_c = \frac{e^2}{4\pi\rho_q \mu k_B T_i} \quad (14)$$

Where: $k_B$is the Boltzmann constant, and T_i the ion temperature. R_f is the dimensionless charging rates due to field transport and R_d is the dimensionless charging rates due to diffusion transport, defined as:

$$R_f = \frac{v_s}{4\varepsilon_0}\left(1 - \frac{v_e}{v_s}\right)^2 \quad (15)$$

$$R_d = \frac{v_e - v_s}{\exp(v_e - v_s) - 1} \quad (16)$$

Where:

$$v_e = \frac{Ze^2}{4\pi\varepsilon_0 r_p k_B T_i} \quad (17)$$

$$v_s = 3w_e \frac{\varepsilon_{r,p}}{\varepsilon_{r,p+2}} \quad (18)$$

$$w_e == \frac{e r_p |E|}{k_B T_i}, \quad (19)$$

where $\varepsilon_{r,p}$ is the relativistic particle permittivity. $f_a$is a function used to relate field charge and diffusion defines as:

$$f_a = \begin{cases} \frac{1}{(w_e + 0.475)^{0.575}} & (w_e \ge 0.525) \\ 1 & (w_e < 0.525) \end{cases} \quad (20)$$

The particle charging process depends on the concentration of gas ions inside the ESP space, which occurs as a result of the ionized gas space between the discharge electrodes and the collection electrodes. The number of ions per cubic meter is several hundred.

2.4. Boundary Conditions

The electric field at the corona electrodes was used as a boundary condition for Poisson's equation:

$$n \bullet \mathrm{E} = E_0 \tag{21}$$

There are other boundary conditions, including V = 0 at the collecting electrodes, also at the inlet and outlet the charge is zero.. The boundary condition for Equation (1) involves in finding the space charge density at ρ_q the corona electrode, using a Lagrange multiplier, so that the imposed potential V_0 is verified

$$V - V_0 = 0\,. \tag{22}$$

In this model both potential and electric field are imposed at the corona electrode. To obtain predictive physical results the value of the electric field at the wire needs to be close enough to the real one. Here, it is used Peek's law:

$$E_0 = 3 \times 10^6 \delta \left(1 + \frac{0.03}{\sqrt{\delta r_i}}\right) \tag{23}$$

3. Geometry and meshing

The performance of the electrostatic precipitator with three internal discharge electrodes, separated by equal distances, was simulated, through the use of the two-dimensional system, and the electrodes are grounded in the form of plates. Figure (1) represents the electrostatic precipitator type (plate wire) used in this article. Simulations and model solutions have been performed in two dimensions to know and calculate the results in all parts of the precipitator, and this allows convergence between them and the practical results. A high DC voltage difference was applied to the inner electrodes while the plate electrode was grounded. The proposed model was solved using the finite element method, by dividing the solution area into small elements that are applicable to all regions. Greater accuracy has been achieved for the elements of the distribution network at the most important areas that occur on the borders, as shown in Figure (1). A corona discharge plasma was created near the inner electrode where the ion density was high as a result of ionization, while the charging process occurred in the area confined between the electrodes and collected on the grounded electrode (plate).

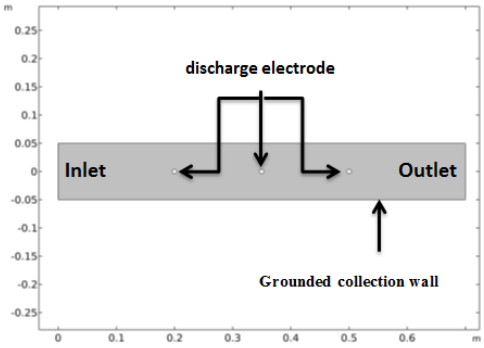

Figure 1: Simulation domain of the electrostatic precipitator.

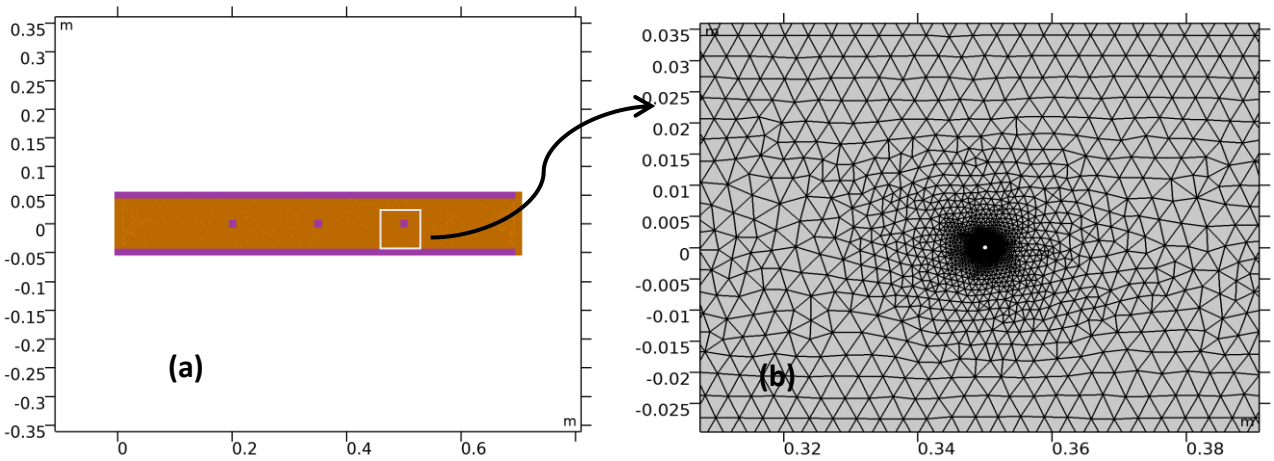

Figure 2 : Mesh structure and geometric parameters. a) The Finite element distribution in 2D for an electrostatic precipitator . b) Shows the zoom of the mesh around the pin electrode and the accuracy of this model's entanglement through some meshes.

4. Results and Discussions

Different voltage values (20, 25, 30, 35) kV were applied to the internal discharge electrodes and their influence on the performance of the precipitator and thus on its efficiency. Simulations were performed using COMSOL Multiphysics 5.5 software. The table (1) below shows the parameters, operating conditions, and inputs for the model used in this paper.

Table.1: the geometry and operational parameters Of the Electrostatic Precipitator.

Name	Expression & Unit	Description
H	0.1[m]	Height
w	0.7[m]	width
rin	0.5 [mm]	Electrode radius
np	3	Electrode number
p	1[atm]	pressure
T	293.15 [k]	temperature
V	20,25,30,35 [KV]	Applied voltage
sp	0.15[m]	Electrode separation

As we mentioned earlier, the electric potential is one of the important parameters of the electrostatic precipitators, and this lies in the dependence of the electric field on it. In this model, the electric potential and electric field are applied to the inner electrode (discharge electrode) and calculated by Equations (21,22,23). Figure (3) represents the voltage distribution inside the precipitator channel for four different values of the applied voltage. The x-axis represents the width of the precipitator and the y-axis its height (see Table 1). It can be noted that the voltage values increase near the inner electrodes and gradually decrease as we approach the collector plates, as shown by the color gradient.

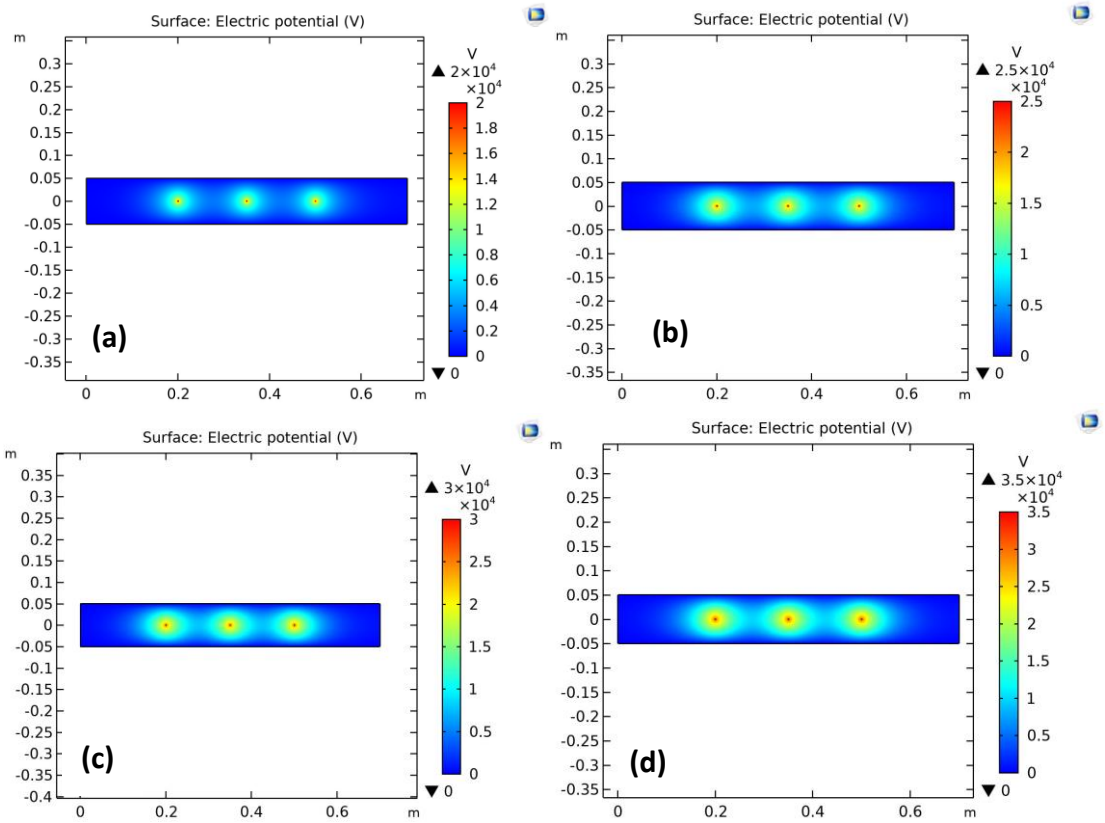

Figure 3: Distribution of the electric potential (V), through the ESP channel for applicable voltages are: (a)20 kV , (b) 25 kV, (c) 30 kV, (d) 35 kV.

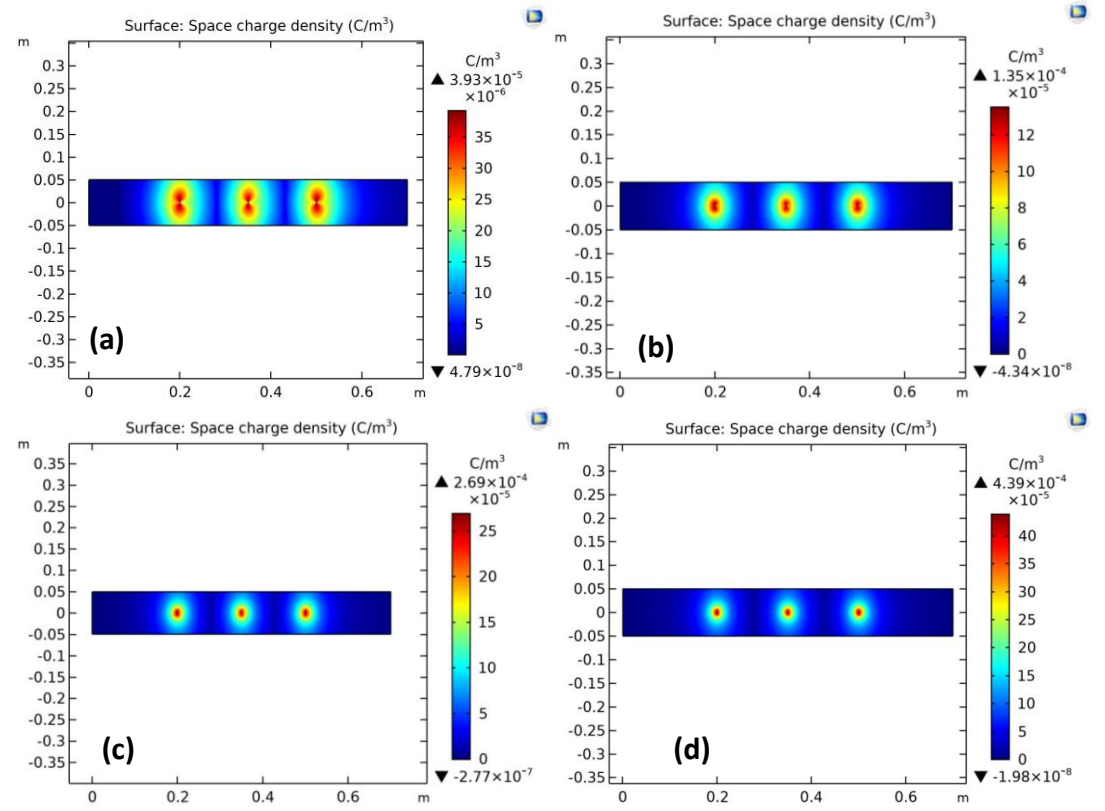

Figure 4: Distribution of space charge density (c/m^3) , through the ESP channel for applicable voltages are: (a)20 kV , (b) 25 kV, (c) 30 kV, (d) 35 kV.

Figure (4) shows the space charge density distribution for four different values of the applied voltage. We notice that the highest value of the charge density is at the highest value of the voltage, and this is what is expected, as the region surrounding the inner electrode is abundant with charges as a result of ionization. a large amount of voltage leads to an acceleration of the free electrons present in the gas close to the discharge electrode.

The results of the current model showed that the fluid velocity was practically not affected by the electrostatic force, as the deflection velocity was always greater than the fluid velocity, especially in the regions of interest. The fluid velocity is an important parameter in the work of the precipitator and it has been calculated from Equations (1, 2). Figure (5) shows the fluid velocity distribution inside the precipitator channel towards the outlet for different applied voltages (four values). It is observed through the figures below of the color gradient that the speed increases with the increase in the applied voltage.

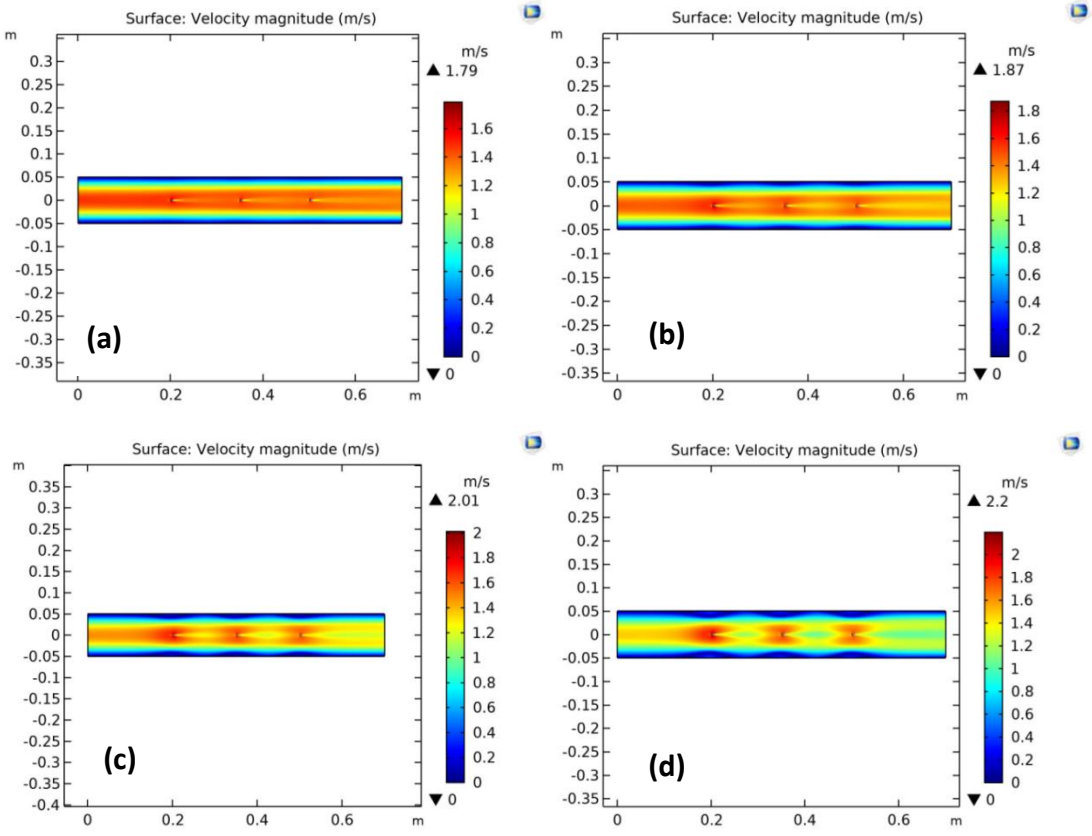

Figure 5: Velocity magnitudes (m/s) through the ESP channel for applicable voltages are: (a)20 kV , (b) 25 kV, (c) 30 kV, (d) 35 kV.

Figures (6, 7, 8) show the trajectories of the particles through the precipitator channel at different voltages and for different particle radii. Figure (6) represents the paths of charged particles with a radius of (0.01 μm). We notice that all particles of this size collect on the collector plates at the highest voltage value. This is fully consistent with the charging process principle indicated earlier, the higher the voltage, the greater the charge potential of the particles. Eventually, the orientation of charged particles of this size increases with the greater ignorance applied to the discharge electrode.

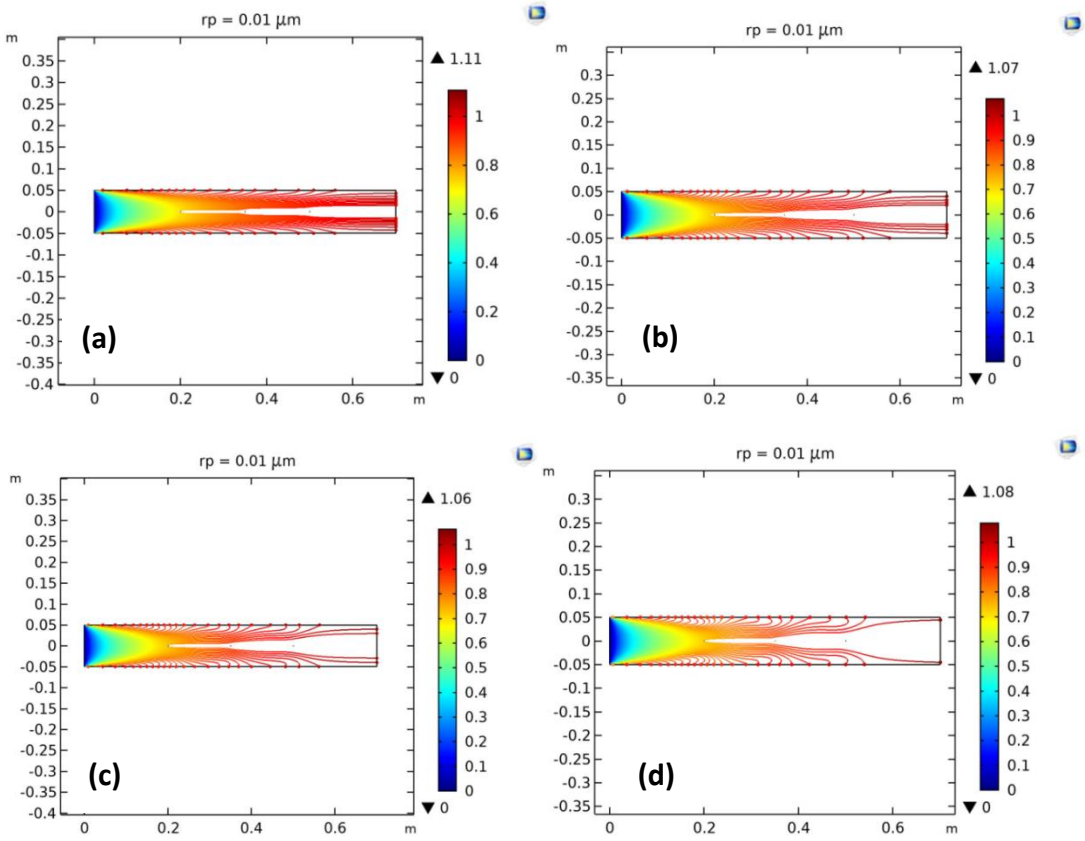

Figure 6: Particle trajectories with the charge number along the trajectory expressed in color for particles with a radius of 0.01 µm, for applicable voltages are: (a)20 kV , (b) 25 kV, (c) 30 kV, (d) 35 kV.

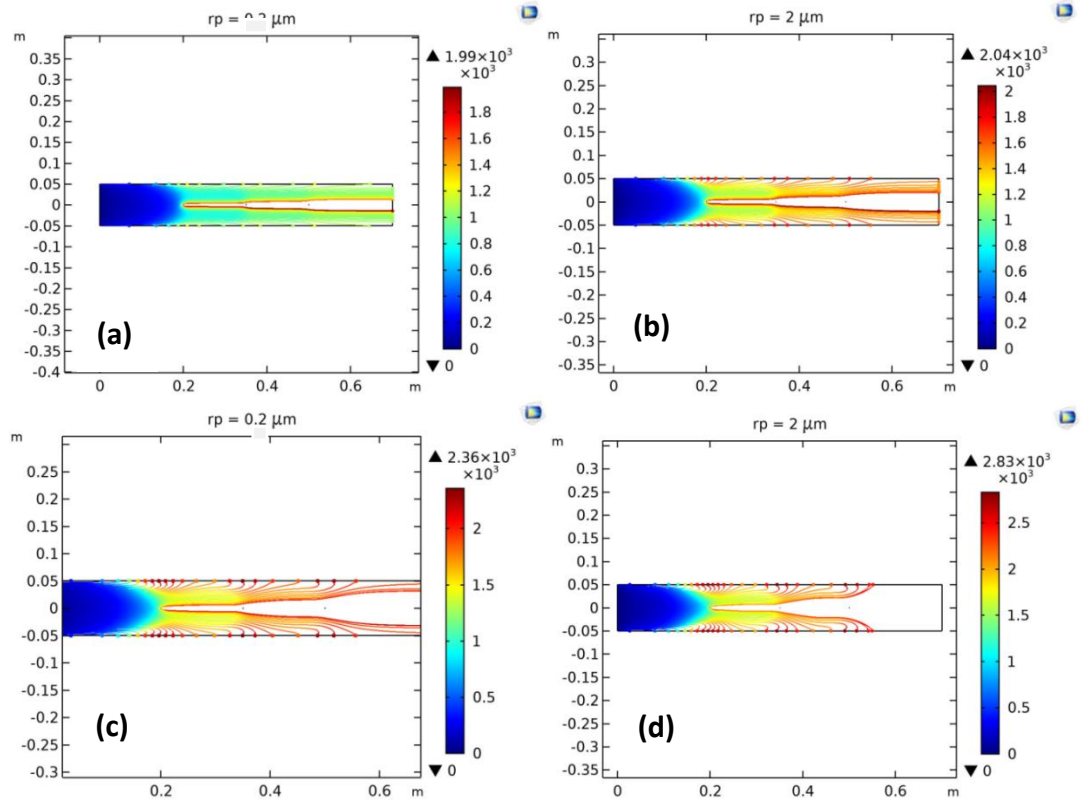

Figure 7: Particle trajectories with the charge number along the trajectory expressed in color for particles with a radius of 2 µm, for applicable voltages are: (a)20 kV , (b) 25 kV, (c) 30 kV, (d) 35 kV.

Figure (7) shows the trajectories of charged particles with radii (2 μm) . It was agreed on the proportionality between the increase in the value of the applied voltage and the internal charging processes. The particles of this size are relatively large, so with an increase in the value of the voltage, the ionization increases, and thus the charge accumulated on the particles increases.

Particles with radii (5 μm) are large among the particles to be charged and directed towards the grounded electrode. Figure (8) shows the trajectories of these particles, and it is also clear that they are completely assembled with the increase in voltage values.

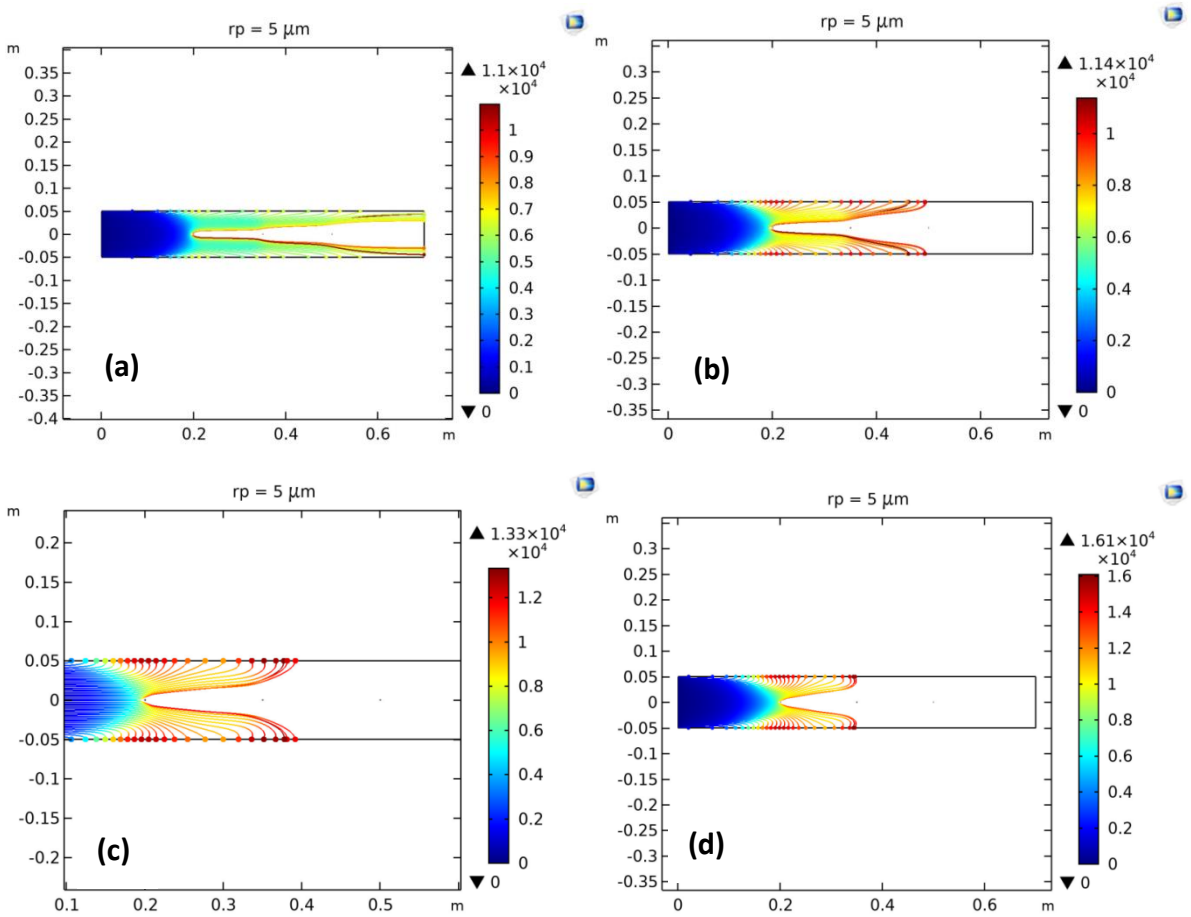

Figure 8: Particle trajectories with the charge number along the trajectory expressed in color for particles with a radius of 5 μm, for applicable voltages are: (a)20 kV , (b) 25 kV, (c) 30 kV, (d) 35 kV.

Figure (9) shows curves for the efficiency of collecting particles according to their diameters. Where the x-axis represents the particle diameters and the y-axis represents the particle collection efficiency. It is clear from the figures below that the efficiency generally increases at the highest voltage. It was also shown that the efficiency increased for small and large diameters. the collection efficiency of size medium particle diameter in an ESP often decreases.

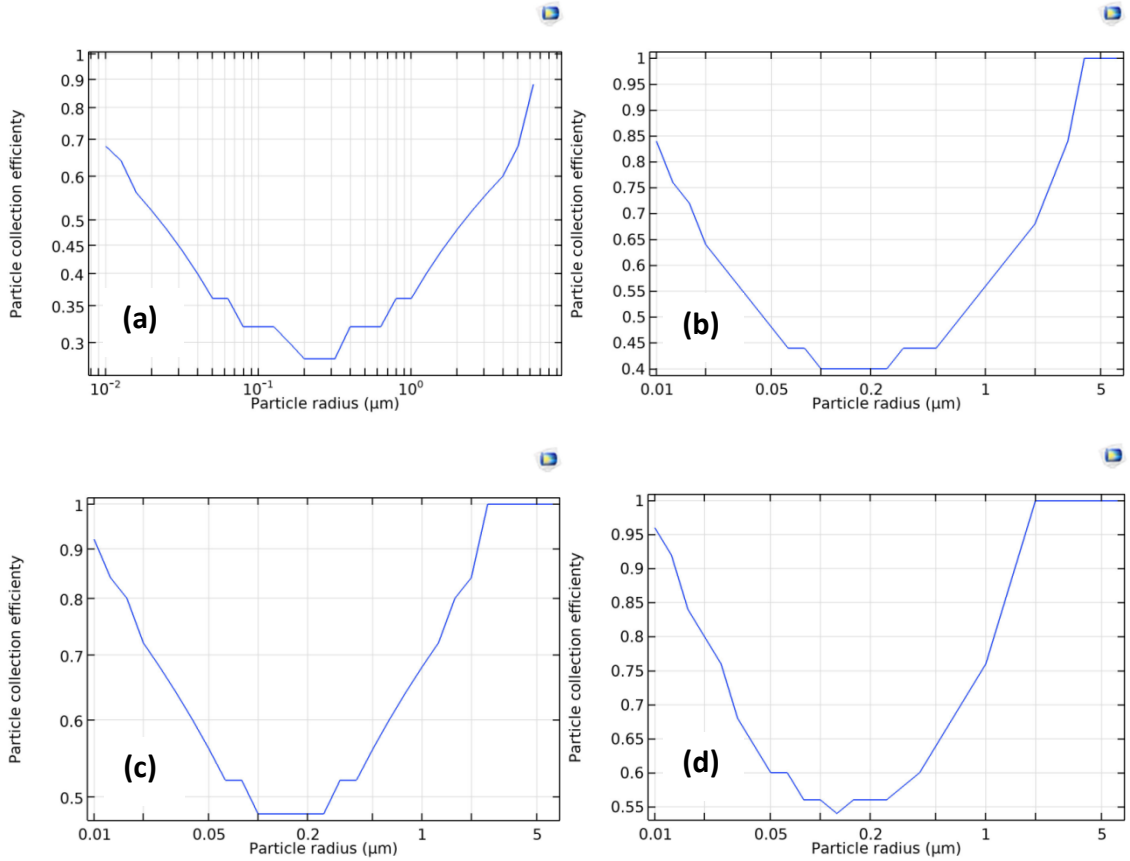

Figure 9: Particle collection efficiency of the electrostatic precipitator, for applicable voltages are: (a)20 kV , (b) 25 kV, (c) 30 kV, (d) 35 kV.

5. Conclusions

In this paper, the effect of the applied voltage on the particle collection efficiency of the electrostatic precipitator was computationally studied. Where four voltage values (20, 25, 30, 35)kV were applied to the inner electrodes and their effect on the particle charging process was studied. The radius of the inner poles was (0.5) mm, the precipitator width (0.7) m, the height (0.1) m, and the fluid flow rate (1) m/s, and operational and geometry conditions were shown in Table 1. Computer simulations were carried out using COMSOL MultiPhysics 5.5 software. The results show that the charging processes increase with the increase in the space charge density and the electric field in the areas surrounding the internal discharge electrodes with the increase in the applied voltage. Finally, the particle collection efficiency of the ESP increases with increasing applied voltage.

References

[1] Tsai, C.-J.; Pui, D.Y.; Editorial, H. Recent advances and new challenges of occupational and environmental health of nanotechnology. J. Nanoparticle Res. 2009, 11, 1–4.

[2] Tsai, C.-J.; Wu, C.-H.; Leu, M.L.; Chen, S.-C.; Huang, C.Y.; Tsai, P.C.; Ko, F.-H. Dustiness test of nanopowders using a standard rotating drum with a modified sampling train. J. Nanoparticle

Res. 2009, 11, 121–131.

[3] Tsai, C.-J.; Huang, C.-Y.; Chen, S.-C.; Ho, C.-E.; Huang, C.-H.; Chen, C.-W.; Chang, C.-P.; Tsai, S.-J.; Ellenbecker, M.J. Exposure assessment of nano-sized and respirable particles at different workplaces. J. Nanoparticle Res. 2011, 13, 4161–4172.

[4] Bango, J.J.; Agostinelli, S.A.; Maroney, M.; Dziekan, M.; Deeb, R.; Duman, G. A Pandemic Early Warning System Decision Analysis Concept Utilizing a Distributed Network of Air Samplers via Electrostatic Air Precipitation. Appl. Sci. 2021, 11, 5308.

[5] Altun, A.F.; Kilic, M. Utilization of electrostatic precipitators for healthy indoor environments. E3S Web Conf. 2019, 111, 02020.

[6] Lin, G.-Y.; Tsai, C.-J. Numerical Modeling of Nanoparticle Collection Efficiency of Single-Stage Wire-in-Plate Electrostatic Precipitators. Aerosol Sci. Technol. 2010, 44, 1122–1130.

[7] Trnka, J.; Janda˘cka, J.; Holub˘cík, M. Improvement of the Standard Chimney Electrostatic Precipitator by Dividing the Flue Gas Stream into a Larger Number of Pipes. Appl. Sci. 2022, 12, 2659.

[8] Wang, W.; Yang, L.; Wu, K.; Lin, C.; Huo, P.; Liu, S.; Huang, D.; Lin, M. Regulation-controlling of boundary layer by multi-wire-tocylinder negative corona discharge. Appl. Therm. Eng. 2017, 119, 438–448.

[9] Lu, Q.; Yang, Z.; Zheng, C.; Li, X.; Zhao, C.; Xu, X.; Gao, X.; Luo, Z.; Ni, M.; Cen, K. Numerical simulation on the fine particle charging and transport behaviors in a wire-plate electrostatic precipitator. Adv. Powder Technol. 2016, 27, 1905–1911.

[10] Dong, M.; Zhou, F.; Zhang, Y.; Shang, Y.; Li, S. Numerical study on fine-particle charging and transport behaviour in electrostatic precipitators. Powder Technol. 2018, 330, 210–218.

[11] Dhayef, H.K.; Khalaf, T. Simulation of a Corona Discharge in a Wire-Duct Electrostatic Precipitator. Project: Plasma Phys. 2022, 21, 4603–4614

[12] F. Kherbouche, Y. Benminoun, A. Tilmatine, A. Zouaghi and N. Zouzou, "Study of a new electrostatic precipitator with asymmetrical wire-to-cylinder configuration for cement particles collection," Journal of Electrostatics, vol. 83, pp. 7-15, 2016.